# CellSP: Module discovery and visualization for subcellular spatial transcriptomics data

Bhavay Aggarwal[1], Saurabh Sinha[1, 2]*.

1 The Wallace H. Coulter Department of Biomedical Engineering, Georgia Institute of Technology, Atlanta, GA, 30332, USA
2 H. Milton Stewart School of Industrial & Systems Engineering, Georgia Institute of Technology, Atlanta, GA, 30318, USA

* Corresponding Author
Corresponding Author-
1. Saurabh Sinha, Email- saurabh.sinha@bme.gatech.edu

## Abstract

Spatially resolved transcriptomics has made it possible to study the subcellular organization of mRNA, a critical aspect of cellular function. However, there is a dearth of analytical tools to identify and interpret the functional significance of subcellular spatial distribution patterns. To address this, we present CellSP, a computational framework for identifying, visualizing, and characterizing consistent subcellular spatial patterns of mRNA. CellSP introduces the concept of "gene-cell modules" to uncover gene sets with non-random subcellular transcript distributions in many cells. CellSP provides intuitive visualizations of the captured patterns and offers functional insights into genes and cells comprising each discovered module. We demonstrate that CellSP reliably identifies functionally significant modules across various tissues and reveals subcellular changes associated with phenotypic variation.

## INTRODUCTION

Spatial transcriptomics (ST) technologies and analytical tools available today offer unprecedented views of gene expression patterns within the intricate tapestry of tissues [1] [2] [3]. At the cutting edge of this technology are single-molecule resolution assays [4] [5] [6], which provide a detailed view of transcript distributions within individual cells, promising to transform our understanding of mRNA localization and its relationship with cellular functions. This relationship has been documented in the literature through anecdotal examples showing that RNA localization to specific subcellular regions may underlie efficient spatial organization of cellular processes [7], rapid local translation in response to external stimuli [8], maintenance of cell polarity [9] [10], facilitation of cell migration [11], coordination of developmental patterning [12], etc. Thus, there is growing recognition of the need to expand our understanding of subcellular RNA localization [13], and the time is ripe for this pursuit, supported by the state-of-the-art subcellular spatial transcriptomics tools.

While experimental techniques have advanced rapidly – enabling, for instance the mapping of individual transcripts of hundreds to thousands of genes in thousands of cells [14] [15] [16] – analytical methods have lagged behind. Available ST-related tools are mostly designed for analysis at the single-cell resolution [17]. More recently, methods targeting subcellular phenomena have emerged [13] [18] [19] [20] that can highlight sub-cellular localization patterns involving single genes or gene pairs, in individual cells. For example, a gene may be annotated as having transcripts localized to cell edges by the BENTO tool [13] or having a "radial" distribution in a cell by the SPRAWL software [19]. Similarly, a gene pair may be found to be significantly colocalized by the InSTAnT toolkit [18], in an individual cell or across many cells. However, when applied to a typical subcellular ST dataset, these tools identify tens of thousands of statistically significant subcellular spatial patterns involving individual genes or gene pairs in individual cells. This overwhelming volume of results imposes a significant interpretive burden, complicating the transition from statistical findings to meaningful and actionable biological insights. The goal of this work is to bridge this gap with an analytical method that identifies the most salient subcellular spatial patterns in an ST data set, along with biological interpretations of those patterns.

An important lesson from decades of transcriptomics data analysis is the concept of gene "module" – a set of genes that share some common pattern of expression. Systematic identification of gene modules [21] followed by statistical enrichment tests [22] is a popular approach to distil a large number of statistical observations into a more compact set of systems-level insights. Inspired by this paradigm, we sought a method to define gene modules with shared subcellular spatial patterns. One simple strategy is to determine if a gene exhibits a specific subcellular localization (e.g., "cell edge" according to BENTO) in many cells, and group together all genes exhibiting the same frequent localization into a module. This strategy is overly

permissive, since two genes annotated with the same frequent localization pattern may not exhibit that common pattern in the same cells. We therefore conceptualized a “gene-cell” module as a set of genes that exhibit the same subcellular pattern in the same cells. However, requiring all genes of a module to exhibit the same subcellular pattern in all module cells is overly restrictive, and will result in fragmented modules. To address this, we adopted a biclustering technique for discovering gene-cell modules from larger collections of genes and gene pairs identified by subcellular pattern discovery tools. This algorithm forms the core of the software presented here, called “CellSP”.

CellSP analyzes single-molecule resolution ST data, identifies significant subcellular spatial distribution patterns at the gene level, and distills them into a compact list of gene-cell modules that typically comprise tens of genes and hundreds of cells. It provides specialized techniques for visualizing such modules and their defining spatial patterns. It uses gene set enrichment analysis to describe the genes comprising the module. Additionally, it uses machine learning classification to distinguish module-associated from other cells in the tissue based on their transcriptomic profiles, identifying genes and biological properties (beyond cell type) that characterize module cells.

We used CellSP to analyze ST data sets from four different studies generated using two different technologies. We present the results of these analyses and provide guidance on interpreting the discovered modules. We identify modules associated with myelination in mouse brain tissues across various technologies and find these modules to exhibit differences linked to Alzheimer’s disease. The reported differences are not necessarily detectable through traditional gene expression analyses. We also find modules related to cell-cell adhesion and axonogenesis, and a closer examination of these modules sheds light on interactions among neighboring cells. Use of CellSP on a cancer data set reveals immune-response related gene-cell modules representing subcellular phenomena specific to cancer versus healthy tissue. In summary, CellSP establishes a robust framework for the systematic detection, visualization and comparison of subcellular transcriptomic patterns, coupled with a statistical characterization of their associated biological functions.

## RESULTS

### Overview of CellSP

CellSP is a tool for analysis of spatial transcriptomics (ST) data at single-molecule resolution (**Figure 1A**). It identifies “gene-cell modules”, where a module is defined as a set of genes exhibiting a specific subcellular spatial distribution pattern (of their transcripts) in a set of cells. Modules are recovered based on statistical criteria and represent the occurrence of interesting, persistent subcellular spatial phenomena in the tissue. There are three main steps involved:

*Step 1 – Subcellular pattern discovery*. Here, the statistical tools SPRAWL [19] and InSTAnT [18] are used to rigorously identify sub-cellular spatial patterns involving individual genes (SPRAWL) or gene pairs (InSTAnT), in each cell (**Figure 1B**). SPRAWL identifies four types of subcellular patterns – peripheral, radial, punctate and central – describing the distribution of a gene’s transcripts within the cell, while InSTAnT tests if transcripts of a gene pair tend to be proximal to each other more often than expected by chance. Patterns of each type are stored in a matrix whose columns represent genes or gene pairs and rows represent cells (**Figure 1C**, left), with entries representing strength of pattern occurrence. Five such matrices are produced, one for each of the four spatial patterns from SPRAWL analysis and one from InSTAnT analysis.

*Step 2 – Module discovery*. Next, a statistical tool called LAS (Large Average Submatrices) [23] is used to analyze each pattern annotation matrix and identify "biclusters", i.e., a subset of rows and columns with a large average value (**Figure 1C**, middle). Each bicluster represents a set of genes or gene pairs that exhibit the same type of sub-cellular pattern in the same set of cells, with statistical significance estimated by a Bonferroni-based score (**Methods**). Biclusters identified in this manner may overlap in terms of rows (cells) and columns (genes/gene pairs), yielding many redundant modules. To address this, CellSP deploys an iterative module-coalescing process where pairs of modules comprising similar sets of cells and genes are combined into larger modules (**Methods**, **Figure 1C**, right). The module discovery step utilizes a parallel computing implementation to accelerate runtime and facilitate the analysis of large datasets.

*Step 3 – Module characterization.* To aid biological interpretation, CellSP reports shared properties of the genes and cells of each discovered module (**Figure 1E**). Genes are characterized using Gene Ontology (GO) enrichment tests, while cells are characterized by their cell type composition if such information is available. To provide a more precise characterization of a module's cells, CellSP trains a machine learning classifier to discriminate those cells from all other cells, using the expression levels of all genes other than the module genes. (Here, it uses a reference scRNA-seq data set, if available, to impute levels of genes missing in the ST data set; see **Methods**.) Genes that are highly predictive in this task are then subjected to GO enrichment tests, furnishing hypotheses about biological processes and pathways that are active specifically in the module cells.

*User experience:* The CellSP tool ingests a single-molecule resolution ST data set in the popular "AnnData" format with cell delineations (**Methods**) and returns a listing of gene-cell modules identified for all five pattern types (peripheral, radial, punctate, central, colocalization). The detailed report of each module includes the type of sub-cellular pattern, identities of genes, number of cells, GO terms characterizing the module genes, cell type composition and GO terms associated with module cells. The latter two are provided depending on the availability of cell type annotations and reference scRNA-seq data (**Methods**), both of which are optional.

*Visualization:* CellSP introduces new techniques for intuitive visualization of subcellular phenomena represented by modules. Here, we outline these visualization methods in general terms, specific examples are provided in subsequent sections. For modules defined by gene pair colocalization, it creates a heatmap showing that colocalization frequencies are higher for module genes versus other genes, and in module cells versus other cells (**Figure 1D**, right). Modules of genes that localize in "central" or "peripheral" pattern are depicted using a density plot of transcript distribution at varying radial locations in an idealized circular cell, averaged over all module cells **(Figure 1D**, middle). Subcellular patterns of types "radial" and "punctate" are depicted using a density plot binned by sectors of an idealized circular cell, aggregated over all module cells by aligning their densest sector (**Figure 1D**, left). In each of these visualizations, a side-by-side visual comparison with non-module genes is provided to underscore the specificity of the pattern to the module genes. Additional visual aids provided in the report include sample cells illustrating the subcellular phenomenon directly, "REVIGO" [24] plots of GO term enrichments, and Uniform Manifold Approximation and Projection (UMAP) [25] as well as spatial plots of module cells.

## CellSP reveals myelination- and axonogenesis-related subcellular spatial phenomena in preoptic area of mouse hypothalamus

In its first demonstrative application, we used CellSP to analyze a MERFISH data set comprising 5,149 cells in the hypothalamic preoptic area (POA) of a mouse brain [26], identifying 38 modules spanning the five pattern types and each module comprising 9 genes and 138 cells on average

(**Figure S1A, Data S1**). Each gene appears in less than four modules on average (**Figure S1B**) and each cell appears in less than three modules on average (**Figure S1C**), indicating a small degree of overlap among the modules. The modules comprise genes enriched in a range of biological processes and cellular components, especially cytoskeleton and cellular structure regulation, neuronal function and development, and metabolic processes (**Data S1**). Note that the underlying subcellular pattern discovery tool InSTAnT reports 358 significant gene pairs (p-value < 1e-3) that colocalize in 35 cells on average, while SPRAWL reports 134 genes having a significant pattern (score threshold = 0.5) in 351 cells on average across the four patterns. The resulting compendium of significant statistical findings reported by these tools, tens of thousands in number, creates a substantial interpretive burden. CellSP effectively distills these patterns into a manageable set of modules, streamlining the crucial step of biological interpretation.

We next illustrate the format in which CellSP reports its discovered modules (**Figure S2**) and how specific biological insights can be gleaned from these. The module “M0_I” consists of the four genes Sgk1 (serum/glucocorticoid regulated kinase 1), Ttyh2 (tweety family member 2), Ermn (ermin, ERM-like protein) and Ndrg1 (N-myc downstream regulated 1), and a set of 332 cells (**Figure 2A**). It was identified using InSTAnT in the pattern discovery step (Step 1, see above), which means that these genes exhibit statistically significant co-localization in the module cells, a selection of which are shown in **Figure 2B**. Notably, the co-localization is observed in varying subcellular regions such as the nucleus, nuclear periphery, cytoplasm and cell membrane. (See **Figure S1E** for more examples.) **Figure 2C** illustrates how CellSP helps visualize a colocalization module, highlighting the specificity of the phenomenon to the module’s genes and cells. The module cells are mostly mature oligodendrocytes (67%, **Figure 2D**) and the module genes are enriched for GO terms such as the molecular function “cytoskeletal protein binding” (p-value = 0.001), the cellular component “myelin sheath” (p-value 0.004) and the biological process “supramolecular fiber organization” (p-value = 0.02) (**Figure 2E**). (Note that cytoskeletal protein binding and supramolecular fiber organization play important roles in formation and maintenance of myelin sheath [27] [28].) Moreover, according to CellSP’s classification-based characterization (Step 3, see above), the module cells are marked by genes enriched for “ensheathment of neurons” (p-value = E-12) (**Figure 2F**). Thus, CellSP analysis suggests a connection between subcellular co-localization of the module and the myelination process in mature oligodendrocytes. A possible interpretation is that the mRNAs of these four genes are captured in the process of being transported to the myelin sheath for local translation, as has been recorded for at least two other myelin biogenesis-related genes, viz., Mbp (Myelin Basic Protein) [29] and Mobp (Myelin Oligodendrocyte Basic Protein) [30]. Interestingly, another CellSP-reported module – “M11_S” – represents a punctate subcellular pattern (**Figure S1D**) involving three of the four above genes, viz., Sgk1, Ttyh2, Ermn, and another myelination-related gene, Gjc3 (gap junction protein gamma 3) that has been shown to localize in myelin sheaths [31].

An example of a module discovered using SPRAWL in the pattern annotation step is “M0_S” (**Figure 3A**), consisting of four genes – Fn1 (fibronectin 1), Slco1a4 (solute carrier organic anion transporter family member 1a4), Rgs5 (regulator of G protein signaling 5), Sema3c (semaphorin 3C) – distributed in a peripheral pattern (**Figure 3B**) in 221 cells. **Figure 3C** illustrates how CellSP helps visualize such a module, revealing the greater tendency of this module’s genes to have peripheral localization, compared with background genes. The module genes are enriched in regulation of axonogenesis (**Figure 3E**) [32] [33] [34], while the module cells, mostly neurons (50% inhibitory and 30% excitatory, **Figure 3D**) are marked by genes associated with cell adhesion (**Figure 3F**), a key process during axonogenesis. The peripheral localization pattern defining the module suggests local translation of proteins that localize in neurites (cell delineations mostly capture somata [35]) or extracellular matrix (ECM). Consistent with this speculation, RGS5 protein is known to exhibit strong synaptic localization [36] [37], while FN1 protein is an

extracellular matrix component [38], supporting the possibility of local translation. Considering the module's statistical association with cell-adhesion functions, we examined the transcript distribution in adjacent pairs of cells and observed that the peripheral localization tends to be at the facing boundaries (**Figure 3G-I**, **Figure S3**), a phenomenon not seen in non-module cells. Putting together the different facets of this module's characterization by CellSP, we hypothesize that the four genes are locally translated into proteins that localize at soma boundaries and perform adhesion-related functions. This may be the case if the module cells, mostly neurons, are actively forming synapses, undergoing neurite outgrowth, etc. [39], which is plausible considering that the preoptic region profiled through these data is an important site of developing neurites [40].

**Subcellular spatial patterns recur across cell types, regions of brain, and measurement technologies**

We next analyzed a large ST data set that profiles a whole mouse brain using Xenium technology [41]. This profiles a panel of 248 genes in 162,033 cells grouped into 50 clusters based on their transcriptomes (**Figure S4**)**.** We used CellSP to analyze each cell cluster separately, as large expression differences across clusters may confound the discovery of subcellular pattern modules, and because we sought to test module reproducibility across varying cellular contexts. CellSP identified ~22 modules per cell cluster, each module comprising 8 genes and 68 cells on average (**Data S2**). Some of the prominent biological characterizations (GO terms) reported for these modules included synaptic processes, myelination, hormone receptor activity, cellular responses to external stimuli, extracellular components, secretory processes and inter-cellular communication.

Closer inspection of these results revealed that modules with certain biological characterizations recur in multiple cell clusters (cell types and/or regions) of the brain. For instance, we observed 36 modules, across 18 different clusters (**Data S3, Figure S6**) to be associated with myelination process, i.e., CellSP reported the GO term "ensheathment of neurons" as enriched (nominal p-value < 0.01) in module genes as well as in marker genes of module cells, for each of these modules. There is substantial overlap in their constituent genes (**Figure 4C**), with the three most frequently recurring constituents being the myelin-associated genes Gjc3, Sox10 (SRY-box transcription factor 10) and Opalin (oligodendrocytic myelin paranodal and inner loop protein) [42] [43] [44]. Gjc3 is known to be expressed in myelinating glial cells [31], Sox10 is a transcription factor responsible for the activation of several myelin-specific genes [45] and Opalin is known to promote oligodendrocyte differentiation and axon myelination [46]. We confirmed that the inclusion of a gene in a module is not a mere reflection of its expression levels in module cells (**Figure S5A**), though higher expression does play a role (**Figure S5B**), in that a gene that is less expressed in a cell is less likely to have its subcellular pattern, if any, detected by a statistical procedure. These myelination-associated modules comprise 3493 cells overall, which are observed across clusters with diverse transcriptomic profiles (**Figure 4A**) and in different brain regions (**Figure 4B**). The shared biological properties of these modules are further elucidated by the numerous other GO terms enrichments common to them (**Figure 4D,E**), including mesenchymal stem cell (MSC) differentiation and oligodendrocyte differentiation. MSCs have the potential to differentiate to or stimulate the maturation of oligodendrocytes [47], the primary myelinating cells.

Another prominent theme in the whole-brain CellSP results was the repeated finding of modules characterized by "GABA-ergic synapse", a GO subcellular localization term. Twenty modules across 14 different cell clusters were reported to have this annotation enriched (p-value < 0.0001) in their constituent genes as well as in expression markers of their member cells (**Figure S7A,B**). These modules were observed in different expression contexts (**Figure 4F**) and physical regions

of the brain (**Figure 4G**), and to exhibit different types of subcellular patterns (**Figure S9, Data S6**). Several genes appear repeatedly as members of these modules, with the most frequent ones being Gad1 (glutamate decarboxylase 1), Gad2 (glutamate decarboxylase 2) and Rab3b (RAB3B, member RAS oncogene family) (**Figure S7C, Figure S8**), which play critical roles in maintaining basal levels of GABA (Gamma-aminobutyric acid), as well as synthesis and vesicle release of GABA in an activity-dependent manner at inhibitory synapses [48] [49] [50]. There is evidence suggesting that GAD2 and RAB3B proteins are localized in presynaptic terminals [49] [51], hinting at an explanation for the subcellular colocalization of their transcripts.

**CellSP-detected modules can be specific to biological conditions**

The analyses above show us that gene-cell modules recovered by CellSP reveal sub-cellular transcriptomic phenomena related to biological processes such as myelination and axonogenesis. This raises the natural question: do these modules also reveal subcellular phenomena that vary under different tissue conditions? To investigate this, we used CellSP on data sets comprising case-control pairs of tissues. The first such analysis involved Xenium data on a kidney cancer (papillary renal cell carcinoma) FFPE sample (**Figure S10A**) and a healthy kidney sample [52]. As in the whole-brain analysis above, we first clustered the cells of each sample based on their transcriptomes and analyzed each cell cluster with CellSP, identifying 11 modules in the cancer sample and 15 modules in the healthy sample (**Data S5, S6**). The cancer modules were mostly (10/11) found in two of the 18 cell clusters (**Figure 5A, Figure S10B**) – Cluster 6 and Cluster 9. Six of these cancer modules comprise genes and cells characterized by CellSP as being immune response-related, with enrichment of GO terms such as “immune response”, “defense response”, “T cell activation”, “positive regulation of leukocyte proliferation”, etc. (**Data S5**).

Examination of the 15 modules in the healthy sample (**Data S6**) suggested that the immune response-related modules found in the cancer sample were specific to it and were not present in the healthy sample. To pursue this observation objectively, we used CellSP visualization routines to contrast a module’s spatial pattern in the module cells (from the cancer sample) versus cells in the other (healthy) tissue sample. As condition-specific gene expression can be a confounder for such analysis, this analysis used a subset of healthy tissue cells that matched the cancer module cells in the expression levels of module genes (**Methods**). **Figures 5B-D** show the cancer-versus-healthy tissue comparison for three of the seven cancer-associated immune-response modules. For instance, module C6_M5_S (**Figure 5B**) comprises a set of 31 genes that are localized centrally in a subset of 22 cells (**Figure S10C**) and was detected in Cluster 6 of the cancer sample (**Figure 5A**). The genes are enriched for the GO term “defense response” (p-value 8.9E-08). As shown in **Figure 5B** (right), the same set of genes lacks this centrally localized distribution of transcripts in expression-matched cells from the healthy sample. A second example is the module C6_M0_S (**Figure 5C**), a set of 24 genes, also enriched in “defense response” (p-value 3.3E-04), that exhibit radial subcellular localization in a set of 18 cells (**Figure S10D**) of Cluster 6. CellSP visualization (**Figure 5C,** left) confirms that the spatial pattern is significantly different between module genes and other genes when examining the module cells. The adjacent panel (**Figure 5C,** right) shows that this prominent contrast is not seen in expression-matched cells from healthy tissue, supporting the cancer-specificity of this module. The third cancer-specific module we highlight here is C6_M3_I (**Figure 5D**), a set of seven genes enriched in the term “T cell activation”, that exhibit significant subcellular colocalization in 66 cells (**Figure S10E**) of Cluster 6. The strength of its spatial pattern in cancer versus healthy tissue is visualized in **Figure 5D**, where the top left quadrant of the heatmap indicates that the module genes have a stronger tendency for pairwise colocalization in the module (cancer) cells compared to expression-matched non-module cells from the healthy sample. (The other quadrants, especially the bottom-right, show that this contrast is not observed for a random subset of non-module genes.) In

summary, CellSP discovers immune-response related gene-cell modules representing significant subcellular patterns that are specific to cancer versus healthy tissue.

**CellSP detects subcellular patterns associated with Alzheimer's Disease in a mouse model**

We next used CellSP to identify gene-cell modules in brains of mouse models of Alzheimer's Disease (AD). For this, we analyzed Xenium data on a coronal section of one hemisphere of TgCRND8 transgenic male mouse brain at three time points (pathological progression stages), as well as wild-type (WT) mouse brain at similar time points [53]. Following the same procedure as above, we clustered cells in each brain sample and used CellSP to find significant modules in each cell cluster, recovering ~11 gene-cell modules per cluster on average (**Figure S11**, **Data S7**). To contextualize these modules with the AD genetics literature, we focused on six genes from the Xenium gene panel implicated in AD risk [54] (**Figure 5E**). We observed the gene Picalm (phosphatidylinositol binding clathrin assembly protein) to appear in many modules in the AD mice, especially in the early and middle time points, significantly more frequently than in WT mice (t-test p-value 0.047) (**Figure S12**). The Picalm protein is responsible for recruiting clathrin and AP-2 to the plasma membrane [55] as part of clathrin-mediated endocytosis, and contributes to clearance of Amyloid beta (Aβ) at the blood brain barrier [56]. It is also linked to processes that are disrupted in AD and is also genetically associated with the disease [57]. We thus speculate that the observed subcellular patterns involving this gene are reflections of the gene's dysfunction in AD mice. We observed another AD risk gene – Trem2 (triggering receptor expressed on myeloid cells 2) – to feature in many CellSP modules (12) in the late-stage AD mouse brain, significantly more than in the other five samples from WT or AD mice (**Figure S13**). This late stage is associated with increase in AD-associated microglial population [58], and Trem2 is primarily expressed in microglia, where it functions as a transmembrane receptor [59] enabling the progression to a mature disease-associated microglia phenotype [58] and is involved in the response to Aβ plaques [60]. Variants in Trem2 gene have been identified as a significant risk factor for late-onset AD [61], suggesting again that the observed gene-cell modules reveal subcellular phenomena reflecting their dysfunction. The four other AD risk genes were found in a few modules overall (**Figure 5E**) and these modules were of similar counts in AD vs. WT mice. We also note that the above AD-associated changes involving Picalm and Trem2 expression, observed at the subcellular spatial level, would not have been detected at the level of overall cellular expression (**Figure S14**).

We next examined the CellSP-detected modules in AD and WT brains with a focus on myelination. Given the reported connection between myelin damage and AD pathology [62]; and building on our earlier identification of myelination-related gene-cell modules in the mouse brain, we investigated whether such modules have any unique characteristics in one phenotypic group compared to the other. We concentrated on all identified modules associated with the GO term "ensheathment of neurons" (nominal p-value < 0.01) and, to identify any characteristics that differentiate these modules between AD and WT, we examined the frequency of myelination-related genes co-occurring in the same module (**Figure 5F**). While most gene pairs show similar co-occurrence statistics between the two groups, the pairs Olig2 (oligodendrocyte transcription factor 2)-Plp1 (proteolipid protein 1) and Olig2-Mobp have a significantly higher co-occurrence in WT brain compared to AD brain (proportion test p-value < 0.05). (Also see **Data S8**). To follow up on these intriguing observations involving Olig2, a gene essential to maturation of oligodendrocytes (the cells responsible for producing myelin), we next identified all genes that co-occur with Olig2 in a group-specific manner (proportion test p-value < 0.05). (The previous analysis was limited to eight select myelination-related genes, including Olig2.) We found 10 such genes (**Figure 5G**, blue bars), nine of which co-occur with Olig2 preferentially in gene-cell modules of the WT brains, and consist of the above-noted genes Plp1, Mobp as well as other

genes linked to myelination, including Opalin and Cnp (2',3'-cyclic nucleotide 3' phosphodiesterase) [46] [63] [64] [65]. This inter-group difference in module composition is most in time points 1 and 2 (**Data S9**) which correspond to periods of continued myelination in the mice brain [66]. These observations suggest that the integrity and functionality of subcellular modules found in WT brains may be impaired in AD brains, reflecting a broader dysfunction in myelination processes in AD [67]. In summary, our myelination-focused examination of CellSP modules points to a potential significance of Olig2 in Alzheimer's disease pathology, highlighting a shift from normal myelination functions in healthy brains.

The specific relationships and insights uncovered here are a glimpse into the dynamics of the subcellular transcriptome during AD progression, not merely a reflection of differential co-expression of genes at the whole cell level. To substantiate this, we repeated the module discovery using co-expression analysis with the popular WGCNA tool [21]. Modules were detected for each cell cluster in each of the six brain samples, as above, except that these were gene co-expression modules rather than CellSP-identified gene-cell modules. These co-expression modules do not show any preferential co-occurrence of Olig2 with any of genes identified above except one – Olig2-Gatm (glycine amidinotransferase) (p-value < 0.05, **Figure 5G**, orange bars). This analysis underscores the ability of CellSP modules to reveal subcellular pattern changes between phenotypic conditions, that may not be discernible at the cellular level.

## DISCUSSION

Spatially resolved transcriptomic data reveal the rich spatial organization of cells and genes in tissues. These revolutionary omics technologies have been accompanied by a plethora of methods that analyze gene expression in the context of cellular neighborhoods and provide informative insights into interactions of cell types and genes. With the increasing popularity of ST techniques of single-molecule resolution, new methods are needed for gene-level analysis at the subcellular scale. At present, there is a lack of understanding of the functional importance of the spatial distribution of transcripts and whether similar distributions repeat across cells. Here, we introduce CellSP, a computational toolkit to identify, analyze and visualize subcellular spatial transcriptomic patterns.

We build upon the concept of gene modules to define gene-cell modules: sets of genes that exhibit consistent spatial patterns across specific groups of cells. To identify these patterns, we leverage and enhance existing tools such as InSTAnT and SPRAWL, and use biclustering for the aggregation of spatial patterns across both genes and cells. To validate the detected patterns, we develop novel visualizations that effectively aggregate spatial patterns over module cells while offering a clear and fair contrast with the background distribution. Additionally, we leverage Gene Ontology (GO) annotations to elucidate the biological functions associated with these spatial modules, providing deeper insights into their relevance and significance.

We use CellSP on data sets from different high-resolution spatial transcriptomics technologies and on various tissues of mouse brain and human kidney. Our analysis of the mouse brain tissues detected modules related to myelination and neuron function, consistently across tissues and technologies. We also discovered differences in myelination related modules in brains from Alzheimer’s Disease mouse models, and showed how cell adhesion-related modules interact which neighboring module cells by localizing module genes at the boundaries of contact.

We compared our approach to the gene module discovery methods implemented in InSTAnT (**Note S1**) and found that CellSP offers significant advantages in terms of efficiency, scalability

(see run-times in **Note S2**, **Data S13**), and user-friendliness. CellSP's biclustering method enables independent detection of modules; however, the heuristic nature of this method can result in variability across different runs. Additionally, while CellSP's visualizations are effective for representing subcellular patterns, they idealize cells as unit circles, which may not accurately depict elongated or irregularly shaped cells.

In developing CellSP, we were inspired by the phenomenon of local translation [68] which requires the mRNA to be transported to precise locations within the cell where they are translated into proteins. This process ensures spatial and temporal precision in protein synthesis. By capturing consistent subcellular patterns, gene-cell modules aim to reveal co-transportation or co-localization of genes that may participate in similar biological functions, providing insights into the spatial organization of cellular processes. CellSP offers a new approach to subcellular spatial transcriptomics data analysis, addressing aspects that traditional differential expression methods are not designed to capture.

## METHODS

### CellSP module discovery algorithm

We utilize the existing tools InSTAnT [18] and SPRAWL [19] for subcellular pattern detection in individual cells. InSTAnT detects gene pair colocalization in single cells, employing the "Proximal Pairs" (PP) test to calculate colocalization p-values for each gene pair in every cell. It also assigns a global colocalization p-value to each gene pair, via the "Conditional Poisson Binomial" (CPB) test, and we use a user-tunable threshold of 1e-3 on this p-value to limit the set of candidate gene pairs. A matrix $M_I$ is constructed to store the PP test p-values with dimensions $n_{cells}$ x $n_{genepairs}$ where $n_{genepairs}$ is the number of candidate gene pairs. We then perform a negative log transformation on this matrix. SPRAWL detects subcellular mRNA localization patterns and classifies them into four categories - peripheral, central, radial, and punctate. Each gene receives a statistical significance score (on a scale of -1 to 1) representing the strength of the spatial pattern in each cell. These scores are stored in four separate matrices $M_{peripheral}, M_{central}, M_{radial}, M_{punctate}$ each with dimensions $n_{cells}$ x $n_{genes}$. We then use the LAS [23] algorithm to perform bi-clustering on each of these matrices. To access the statistical significance of a bicluster, LAS uses a Gaussian null model for the observed data. The significance score is derived from a Bonferroni-corrected p-value, which accounts for the bicluster's size and the average value of its entries. The LAS algorithm searches iteratively for submatrices or biclusters with high average values and subsequently removes the influence of selected submatrix from the original data matrix. The search process is repeated till the desired number of submatrices are retrieved or until no significant submatrices are found. The reported submatrices are what we call modules. Due to the heuristic nature of this algorithm, some rows (cells) and columns (genes/gene-pairs) that have values similar to those of a reported module, may not be included in the module or might end up in a separate module. To mitigate information loss and reduce redundancy across reported modules, we implement a two-step module expansion process:

1. Cell Expansion – For each module, we iterate through all cells and add a cell to the module if the cell's average value across the module's genes exceeds the original module's average value.
2. Module Aggregation – For every pair of modules, we calculate the overlap coefficient (**Equation 1**) for their genes. If the overlap coefficient exceeds 0.667 and the merged

significance score surpasses the module significance threshold, the two modules are merged, with the new module comprising the union of their genes and cells. This process is repeated iteratively until no further mergers are possible. This expansion step is useful to reduce the number of modules detected and combine modules of similar composition into one. This step is made optional.

$$Overlap(A, B) = \frac{|A \cap B|}{min(|A|, |B|)} \quad (1)$$

In the final reported list of gene-cell modules, two modules may comprise overlapping sets of cells, allowing the same cells to be part of multiple modules, defined by different sets of genes (**Figure 1**). Modules detected from the SPRAWL-derived matrices $M_{peripheral}, M_{central}, M_{radial}, M_{punctate}$ are reported as one group (their identifiers have the suffix "_S" and a unique numeric prefix), while modules detected from the InSTAnT-derived matrix $M_I$ are reported as another group (identifiers with suffix "_I" and a unique numeric prefix).

**Module Characterization**

To investigate factors (other than cell types) that underlie or are associated with subcellular spatial phenomena, CellSP performs a two-level characterization of the detected modules using gene set enrichment analysis and predictive modeling.

*Module Gene Characterization*: The biological functions associated with module genes are characterized using PantherDB [69] for gene enrichment analysis. For each module, the module genes are used as the query gene set, while the gene panel of the ST assay serves as the background set. This analysis identifies pathways, biological processes, and molecular functions enriched in module genes.

*Module Cell Characterization*: To characterize the cells in each module, CellSP trains a classifier to distinguish between module cells (positive set) and all other cells (negative set). Each cell's gene expression profile (total transcript count of each gene in that cell) is used as the cell's feature vector, i.e., this is not a spatially resolved featurization. Since an ST assay of single-molecule resolution typically profiles a limited number of genes, the number of features is relatively modest. To address this, CellSP uses the Tangram tool [70] to impute the expression of additional genes in each cell of the ST data using scRNA-seq data of the same tissue. The imputation process expands the gene set significantly, increasing the number of features from a few hundred (in the original ST data) to several thousand. We construct an extended gene expression matrix by retaining the original expression values for genes present in the ST panel and incorporating the imputed expression values for genes absent from the panel. The extended gene expression matrix is used to train a Random Forest classifier of module cells. The top 20 most informative genes are identified based on their feature importance, which is quantified using SHAP [71] [72]. These genes, along with any other genes that exhibit a high Pearson correlation ($r > 0.98$) with them, are designated as "marker genes" of the module cells. These genes are then subjected to gene set characterization PantherDB to identify pathways, biological processes, and molecular functions that characterize the module's cells.

**Module Pattern Visualization**

To help visualize modules defined by the five types of subcellular spatial patterns (four types identified by SPRAWL and colocalization patterns identified by InSTAnT), we developed three complementary plotting techniques.

SPRAWL detects localization patterns (peripheral, central, radial or punctate) for each gene in each cell. To aggregate these spatial localization patterns across many cells, CellSP transforms each cell into a uniform representation within a unit circle. This transformation is achieved using the smallest enclosing circle algorithm [73] to identify the smallest circle enclosing all transcripts in the cell. The circle is then centered at the origin and scaled to have a unit radius. For “central” and “peripheral” patterns, the unit circle is divided into C (defaults to 5) concentric rings, and the density of module genes within each ring is calculated. These densities are then averaged across all cells of the module. A similar visualization is constructed for all non-module genes in the same module cells and the two plots are placed side-by-side. For modules displaying “central” patterns, we expect the highest densities in the innermost rings, while “peripheral” patterns are anticipated to exhibit higher densities in the outermost rings.

For modules defined by “punctate” or “radial” patterns, the unit circle representing an idealized view of a cell is divided into S (defaults to 10) sectors. Gene transcript density is computed in each sector for module and non-module genes separately. To account for the directional variability of these patterns, each cell’s idealized circle view is rotated such that the sector with the maximum density aligned with 0°. Following this alignment, densities are aggregated across cells by calculating mean densities for each sector. In this framework, module genes are expected to concentrate primarily in the 1$^{st}$ sector, while non-module genes are anticipated to exhibit more uniform distributions across sectors. Density distributions (across sectors) for module genes and non-module genes are plotted on top of each other, in different colors.

InSTAnT detects colocalized gene pairs as those whose transcripts are in close proximity (within distance d) of each other. To visualize such patterns aggregated over cells, CellSP first constructs a d-radius neighborhood graph of transcripts for each module cell, calculates the number of neighboring transcript pairs for each pair of module genes and sums these counts across all module cells, thus obtaining a “proximity score” for that gene pair aggregating information across module cells. This process is then repeated over non-module cells to obtain a proximity score of the same gene pair but now aggregating information from non-module cells. The proximity enrichment score of the gene pair is then defined as the log ratio of proximity scores from module cells and non-module cells. High positive values of the proximity enrichment score indicate that the gene pair exhibits greater colocalization in module cells to a greater extent compared to non-module cells. To add further contrast, a randomly selected set of non-module (“control”) genes (equal in count to the module genes) is included in the visualization: a heatmap is constructed whose rows and columns represent module genes and the selected control genes, and values depict proximity enrichment scores of gene pairs. The upper-left quadrant corresponds to pairs of module genes, the lower-right quadrant to pairs of control genes, and the remaining two quadrants correspond to a module gene paired with a non-module gene.

**Gene Set Enrichment Visualization**

CellSP provides the ability to visualize the gene set enrichment reports generated by PantherDB using Revigo [24]. Revigo summarizes lists of GO terms by clustering them based on their semantic similarity, identifying representative terms. These terms are visualized as circles in a scatterplot, where circle size reflects the gene set size and color intensity indicates statistical significance, with darker colors representing higher significance. This visualization highlights the importance, similarity, and uniqueness of terms, making it easier to interpret enrichment results.

To aggregate Revigo plots across multiple detected modules (**Figure 4D,E**, this is not a standard functionality of CellSP), we first collected all GO terms with a p-value below 1e-2 across the modules. In cases of duplicate terms, the term with the most significant p-value was retained. This aggregated list of significant terms was then processed through Revigo, which calculated the

principal component analysis (PCA) values for each term. Using these PCA coordinates, we generated a 2D histogram to visualize the aggregated GO terms across modules. The PCA values determined the positions of the bins, and the frequency of each term's occurrence in module enrichment analyses was represented by the color intensity of the corresponding bin. This visualization highlights the most commonly enriched biological themes across modules while preserving the semantic relationships among GO terms.

**Cross-Condition Module Comparison**

*Human Kidney Dataset*: To compare the detected modules between conditions in the Human Kidney dataset, we assessed whether the subcellular patterns of modules from the cancer condition were present in the control tissue. We first performed min-max normalization of gene expression values for both the control and cancer datasets independently. For a gene-cell module detected in the cancer dataset, we calculated the total gene expression of module genes in each module cell and determined their minimum $P_{min}$ and maximum $P_{max}$ as percentiles in the population of total gene expression of all cells in the cancer dataset. Using these percentiles, we identified cells from the control dataset with total gene expression between $P_{min}$ and $P_{max}$ percentile of the population of control cells. Thus, we identified a subset of the control cells whose total expression is similar to the module cells (which belong to the cancer data set). Subcellular patterns of module genes were then visualized in these control cells and compared to the patterns in the module cells from the cancer dataset.

*Mouse Alzheimer's Disease Dataset*: To identify changes in functionally similar (myelination-related) modules across conditions (AD model mice and WT mice), we asked whether two sets of modules (one set from each condition) differ in their gene composition. One way to answer this is based on how many modules in each condition include a specific gene, and whether the gene's frequency of inclusion is different between conditions. This approach was used for **Figure 5G**. A complementary approach is based on how many modules in each condition include a specific gene pair and comparing the proportion of such modules between conditions using a one-sided proportion test [74]. The test statistic for the proportion test is given by:

$$z = \frac{\widehat{p_1} - \widehat{p_2}}{\sqrt{\hat{p}(1-\hat{p})\left(\frac{1}{n_1} + \frac{1}{n_2}\right)}} \qquad (2)$$

where $\hat{p}_1$ is the proportion for group 1, $\hat{p}_2$ is the proportion for group 2, $\hat{p}$ is the pooled proportion and $n_1$, $n_2$ are the sample sizes for group 1 and 2 respectively.

**Comparison with traditional analysis methods**

To compare insights generated by our approach against traditional methods, we performed differential expression analysis and co-expression network analysis on the datasets. For differential expression analysis, we utilized Scanpy [75] to apply the Wilcoxon rank-sum test, comparing gene expression between the two conditions under investigation. This provided insights into genes with significantly altered expression levels across conditions.

For co-expression network analysis, we employed WGCNA [21] using the PyWGCNA framework [76]. Similar to our approach using CellSP, WGCNA was run independently for each cell cluster in the dataset. WGCNA assigns a module identity (class label) to each gene within a cluster based on its co-expression patterns. We used these module identities to calculate the frequency with

which a gene pair is assigned to the same module across the dataset. These frequencies were then compared between the conditions using a one-sided proportion test to assess condition-specific co-expression relationships.

**CellSP User Guide**

CellSP provides flexible and tunable parameters that allow users to adapt analyses to their specific datasets and objectives. For InSTAnT, the distance threshold (d) is typically set to approximately 5% of the average cell diameter. The significance threshold (α) is set to be 1e-5 by default, following the original implementation. However, if this results in too few significant gene pairs (< 250 gene-pairs), we recommend relaxing the threshold to 1e-3 or lower. To manage computational complexity, an additional parameter, K, allows users to select the top K gene pairs for further analysis. For SPRAWL, we adapted the original scripts into CellSP to enable parallelization and use the default parameters. Similarly, LAS scripts from the implementation available in biclustlib [77] were parallelized and integrated into CellSP. LAS includes two primary adjustable parameters: N and RS. The parameter N determines the number of modules to search and is set to a default value of 10, which can be adjusted empirically based on the dataset and research goals. The parameter RS specifies the number of randomized searches performed to enhance the quality of the biclusters. By default, RS is set to 50,000; however, for larger datasets (e.g., > 200 genes or > 10,000 cells), we recommend reducing this value to balance computational demands while maintaining reasonable bicluster quality. Visualization in CellSP is also highly customizable. Users can fine-tune the representation of subcellular patterns using parameters such as the number of concentric circles (C), the number of sectors (S), and the distance threshold (d). These settings provide flexibility in highlighting key spatial patterns. Details for the specific parameters used in each analysis can be found in **Data S10**.

## DATA AVAILABILITY

The MERFISH dataset for the Mouse Preoptic Hypothalamus region [26] was obtained through direct communication with Dr. Jeffrey Moffitt. After excluding cells labeled with ambiguous cell types, the dataset comprises 5,149 cells distributed across 9 distinct cell types, with a gene panel of 135 genes.

The Xenium datasets are publicly available at 10x Genomics Datasets. We used the "Fresh Frozen Mouse Brain for Xenium Explorer Demo" [41], "Human Kidney Preview Data" [52], and the "Xenium In Situ Analysis of Alzheimer's Disease Mouse Model Brain Coronal Sections from One Hemisphere Over a Time Course" [53] datasets for the mouse brain, human kidney, and Alzheimer's disease experiments, respectively. The Mouse Brain dataset contains 162,033 cells grouped into 50 clusters based on the expression profiles of 248 genes. The Human Kidney dataset comprises 56,509 cells grouped into 19 clusters in the cancer tissue and 97,546 cells grouped into 21 clusters in the control tissue. The gene panel includes 377 genes. The Mouse Alzheimer’s dataset includes six tissue samples from two conditions—Wild Type and Alzheimer’s (TgCRND8 mouse model)—at three timepoints (2.5 months, 5.7 months, and 13+ months). The Alzheimer’s samples contain 53,908, 58,681, and 61,435 cells across the timepoints, while the Wild Type samples contain 58,230, 58,685, and 59,933 cells, with a gene panel of 347 genes. Additionally, we used the Mouse Brain coronal hemisphere dataset from CosMx, which is also publicly available. This dataset includes 48,180 cells, grouped into 45 cell types, with a panel of 950 genes.

## CODE AVAILABILITY

CellSP is open source and available at https://github.com/bhavaygg/cellSP.

**ACKNOWLEDGEMENTS**

We thank Abhishek Ojha for his help in designing the statistical tests. Funding: This work was supported by the National Institutes of Health (R35GM131819 to S.S.), and Georgia Institute of Technology (Wallace H. Coulter Distinguished Faculty Chair: S.S.)

673 **REFERENCES**

674

[1] K. R. Maynard, L. Collado-Torres, L. M. Weber, C. Uytingco, B. K. Barry, S. R. Williams, J. L. Catallini, M. N. Tran, Z. Besich, M. Tippani and others, "Transcriptome-scale spatial gene expression in the human dorsolateral prefrontal cortex," *Nature neuroscience,* vol. 24, p. 425–436, 2021.

[2] B. Watson, B. Paul, L. Amir-Zilberstein, A. Segerstolpe, R. Rahman, A. Shih, J. Deguine, R. Xavier, J. R. Moffitt and A. C. Mullen, "Spatial transcriptomics of healthy and fibrotic human liver at single-cell resolution," *bioRxiv,* p. 2024–02, 2024.

[3] P. Cadinu, K. N. Sivanathan, A. Misra, R. J. Xu, D. Mangani, E. Yang, J. M. Rone, K. Tooley, Y.-C. Kye, L. Bod and others, "Charting the cellular biogeography in colitis reveals fibroblast trajectories and coordinated spatial remodeling," *Cell,* vol. 187, p. 2010–2028, 2024.

[4] H. Shi, Y. He, Y. Zhou, J. Huang, K. Maher, B. Wang, Z. Tang, S. Luo, P. Tan, M. Wu and others, "Spatial atlas of the mouse central nervous system at molecular resolution," *Nature,* vol. 622, p. 552–561, 2023.

[5] E. N. Farah, R. K. Hu, C. Kern, Q. Zhang, T.-Y. Lu, Q. Ma, S. Tran, B. Zhang, D. Carlin, A. Monell and others, "Spatially organized cellular communities form the developing human heart," *Nature,* vol. 627, p. 854–864, 2024.

[6] M. Zhang, X. Pan, W. Jung, A. R. Halpern, S. W. Eichhorn, Z. Lei, L. Cohen, K. A. Smith, B. Tasic, Z. Yao and others, "Molecularly defined and spatially resolved cell atlas of the whole mouse brain," *Nature,* vol. 624, p. 343–354, 2023.

[7] C. E. Holt and S. L. Bullock, "Subcellular mRNA localization in animal cells and why it matters.," *Science (New York, N.Y.),* vol. 326, no. 5957, p. 1212–1216, November 2009.

[8] D. Wang, Z. Zhang, Y. Jiang, Z. Mao, D. Wang, H. Lin and D. Xu, "DM3Loc: multi-label mRNA subcellular localization prediction and analysis based on multi-head self-attention mechanism," *Nucleic acids research,* vol. 49, p. e46–e46, 2021.

[9] T. Schuster, A. Amoah, A. Vollmer, G. Marka, J. Niemann, M. Saçma, V. Sakk, K. Soller, M. Vogel, A. Grigoryan and others, "Quantitative determination of the spatial distribution of components in single cells with CellDetail," *Nature Communications,* vol. 15, p. 10250, 2024.

[10] J. Barr, K. V. Yakovlev, Y. Shidlovskii and P. Schedl, "Establishing and maintaining cell polarity with mRNA localization in Drosophila.," *BioEssays : news and reviews in molecular, cellular and developmental biology,* vol. 38, no. 3, p. 244–253, March 2016.

[11] M. Dermit, M. Dodel, F. C. Y. Lee, M. S. Azman, H. Schwenzer, J. L. Jones, S. P. Blagden, J. Ule and F. K. Mardakheh, "Subcellular mRNA Localization Regulates Ribosome Biogenesis in Migrating Cells.," *Developmental cell,* vol. 55, no. 3, p. 298–313.e10, November 2020.

[12] R. M. Parton, A. Davidson, I. Davis and T. T. Weil, "Subcellular mRNA localisation at a glance," *Journal of cell science,* vol. 127, p. 2127–2133, 2014.

[13] C. K. Mah, N. Ahmed, N. A. Lopez, D. C. Lam, A. Pong, A. Monell, C. Kern, Y. Han, G. Prasad, A. J. Cesnik and others, "Bento: a toolkit for subcellular analysis of spatial transcriptomics data," *Genome Biology,* vol. 25, p. 82, 2024.

[14] K. H. Chen, A. N. Boettiger, J. R. Moffitt, S. Wang and X. Zhuang, "Spatially resolved, highly multiplexed RNA profiling in single cells," *Science,* vol. 348, p. aaa6090, 2015.

[15] C.-H. L. Eng, M. Lawson, Q. Zhu, R. Dries, N. Koulena, Y. Takei, J. Yun, C. Cronin, C. Karp, G.-C. Yuan and others, "Transcriptome-scale super-resolved imaging in tissues by RNA seqFISH+," *Nature,* vol. 568, p. 235–239, 2019.

[16] X. Wang, W. E. Allen, M. A. Wright, E. L. Sylwestrak, N. Samusik, S. Vesuna, K. Evans, C. Liu, C. Ramakrishnan, J. Liu, G. P. Nolan, F.-A. Bava and K. Deisseroth, "Three-dimensional intact-tissue sequencing of single-cell transcriptional states.," *Science (New York, N.Y.),* vol. 361, no. 6400, July 2018.

[17] K. Dong and S. Zhang, "Deciphering spatial domains from spatially resolved transcriptomics with an adaptive graph attention auto-encoder," *Nature communications,* vol. 13, p. 1739, 2022.

[18] A. Kumar, A. W. Schrader, B. Aggarwal, A. E. Boroojeny, M. Asadian, J. Lee, Y. J. Song, S. D. Zhao, H.-S. Han and S. Sinha, "Intracellular spatial transcriptomic analysis toolkit (InSTAnT)," *Nature communications,* vol. 15, p. 7794, 2024.

[19] R. Bierman, J. M. Dave, D. M. Greif and J. Salzman, "Statistical analysis supports pervasive RNA subcellular localization and alternative 3'UTR regulation," *eLife,* vol. 12, p. RP87517, 2024.

[20] F. C. Walter, O. Stegle and B. Velten, "FISHFactor: a probabilistic factor model for spatial transcriptomics data with subcellular resolution," *Bioinformatics,* vol. 39, p. btad183, 2023.

[21] P. Langfelder and S. Horvath, "WGCNA: an R package for weighted correlation network analysis," *BMC bioinformatics,* vol. 9, p. 1–13, 2008.

[22] A. Subramanian, P. Tamayo, V. K. Mootha, S. Mukherjee, B. L. Ebert, M. A. Gillette, A. Paulovich, S. L. Pomeroy, T. R. Golub, E. S. Lander and others, "Gene set enrichment analysis: a knowledge-based approach for interpreting genome-wide expression profiles," *Proceedings of the National Academy of Sciences,* vol. 102, p. 15545–15550, 2005.

[23] A. A. Shabalin, V. J. Weigman, C. M. Perou and A. B. Nobel, "Finding large average submatrices in high dimensional data," *The Annals of Applied Statistics,* p. 985–1012, 2009.

[24] F. Supek, M. Bošnjak, N. Škunca and T. Šmuc, "REVIGO summarizes and visualizes long lists of gene ontology terms," *PloS one,* vol. 6, p. e21800, 2011.

[25] L. McInnes, J. Healy and J. Melville, "Umap: Uniform manifold approximation and projection for dimension reduction," *arXiv preprint arXiv:1802.03426,* 2018.

[26] J. R. Moffitt, D. Bambah-Mukku, S. W. Eichhorn, E. Vaughn, K. Shekhar, J. D. Perez, N. D. Rubinstein, J. Hao, A. Regev, C. Dulac and others, "Molecular, spatial, and functional single-cell profiling of the hypothalamic preoptic region," *Science,* vol. 362, p. eaau5324, 2018.

[27] H. Wang, A. Tewari, S. Einheber, J. L. Salzer and C. V. Melendez-Vasquez, "Myosin II has distinct functions in PNS and CNS myelin sheath formation.," *The Journal of cell biology,* vol. 182, no. 6, p. 1171–1184, September 2008.

[28] H. Inouye, J. Liu, L. Makowski, M. Palmisano, M. Burghammer, C. Riekel and D. A. Kirschner, "Myelin organization in the nodal, paranodal, and juxtaparanodal regions revealed by scanning x-ray microdiffraction," *PLoS One,* vol. 9, p. e100592, 2014.

[29] L. S. Laursen, C. W. Chan and C. ffrench-Constant, "Translation of myelin basic protein mRNA in oligodendrocytes is regulated by integrin activation and hnRNP-K," *Journal of Cell Biology,* vol. 192, p. 797–811, February 2011.

[30] R. Gould and S. Brady, "Identifying mRNAs Residing in Myelinating Oligodendrocyte Processes as a Basis for Understanding Internode Autonomy.," *Life (Basel, Switzerland),* vol. 13, no. 4, April 2023.

[31] B. M. Altevogt, K. A. Kleopa, F. R. Postma, S. S. Scherer and D. L. Paul, "Connexin29 is uniquely distributed within myelinating glial cells of the central and peripheral nervous systems.," *The Journal of neuroscience : the official journal of the Society for Neuroscience,* vol. 22, no. 15, p. 6458–6470, August 2002.

[32] E. Koncina, L. Roth, B. Gonthier and D. Bagnard, "Role of semaphorins during axon growth and guidance," *Axon growth and guidance,* p. 50–64, 2007.

[33] C. Liu, Q. Hu, J. Jing, Y. Zhang, J. Jin, L. Zhang, L. Mu, Y. Liu, B. Sun, T. Zhang, Q. Kong, G. Wang, D. Wang, Y. Zhang, X. Liu, W. Zhao, J. Wang, T. Feng and H. Li, "Regulator of G protein signaling 5 (RGS5) inhibits sonic hedgehog function in mouse cortical neurons.," *Molecular and cellular neurosciences,* vol. 83, p. 65–73, September 2017.

[34] D. A. Tonge, H. T. de Burgh, R. Docherty, M. J. Humphries, S. E. Craig and J. Pizzey, "Fibronectin supports neurite outgrowth and axonal regeneration of adult brain neurons in vitro.," *Brain research,* vol. 1453, p. 8–16, May 2012.

[35] V. Petukhov, R. J. Xu, R. A. Soldatov, P. Cadinu, K. Khodosevich, J. R. Moffitt and P. V. Kharchenko, "Cell segmentation in imaging-based spatial transcriptomics," *Nature Biotechnology,* vol. 40, p. 345–354, October 2021.

[36] P. J. Thul, L. Åkesson, M. Wiking, D. Mahdessian, A. Geladaki, H. Ait Blal, T. Alm, A. Asplund, L. Björk, L. M. Breckels, A. Bäckström, F. Danielsson, L. Fagerberg, J. Fall, L. Gatto, C. Gnann, S. Hober, M. Hjelmare, F. Johansson, S. Lee, C. Lindskog, J. Mulder, C. M. Mulvey, P. Nilsson, P. Oksvold, J. Rockberg, R. Schutten, J. M. Schwenk, Å. Sivertsson, E. Sjöstedt, M. Skogs, C. Stadler, D. P. Sullivan, H. Tegel, C. Winsnes, C. Zhang, M. Zwahlen, A. Mardinoglu, F. Pontén, K. von Feilitzen, K. S. Lilley, M. Uhlén and E. Lundberg, "A subcellular map of the human proteome.," *Science (New York, N.Y.),* vol. 356, no. 6340, May 2017.

[37] The Human Protein Atlas, *RGS5.*

[38] J. Wang, L. Yin and Z. Chen, "Neuroprotective role of fibronectin in neuron-glial extrasynaptic transmission.," *Neural regeneration research,* vol. 8, no. 4, p. 376–382, February 2013.

[39] H. Togashi, T. Sakisaka and Y. Takai, "Cell adhesion molecules in the central nervous system.," *Cell adhesion & migration,* vol. 3, no. 1, p. 29–35, 2009.

[40] J. Biran, M. Tahor, E. Wircer and G. Levkowitz, "Role of developmental factors in hypothalamic function.," *Frontiers in neuroanatomy,* vol. 9, p. 47, 2015.

[41] 10x Genomics, "Fresh Frozen Mouse Brain Replicates," *In Situ Gene Expression dataset analyzed using Xenium Onboard Analysis 1.0.2,* 2023, Jan 22.

[42] C. K. Abrams, "Diseases of connexins expressed in myelinating glia.," *Neuroscience letters,* vol. 695, p. 91–99, March 2019.

[43] T. Turnescu, J. Arter, S. Reiprich, E. R. Tamm, A. Waisman and M. Wegner, "Sox8 and Sox10 jointly maintain myelin gene expression in oligodendrocytes," *Glia,* vol. 66, pp. 279-294, 2018.

[44] R. Tang, J. Vargas-Medrano, E. Ramos, P. Thompson and B. Gadad, "Gene Expression Analysis of CCL2, MOBP and OPALIN in Major Depressive Disorder and Suicidality (P5-6.005)," *Neurology,* vol. 98, p. 3266, 2022.

[45] J. Hornig, F. Fröb, M. R. Vogl, I. Hermans-Borgmeyer, E. R. Tamm and M. Wegner, "The transcription factors Sox10 and Myrf define an essential regulatory network module in differentiating oligodendrocytes," *PLoS genetics,* vol. 9, p. e1003907, 2013.

[46] O. de Faria Jr, A. S. Dhaunchak, Y. Kamen, A. D. Roth, T. Kuhlmann, D. R. Colman and T. E. Kennedy, "TMEM10 promotes oligodendrocyte differentiation and is expressed by oligodendrocytes in human remyelinating multiple sclerosis plaques," *Scientific reports,* vol. 9, p. 3606, 2019.

[47] S. George, M. R. Hamblin and H. Abrahamse, "Differentiation of mesenchymal stem cells to neuroglia: in the context of cell signalling," *Stem cell reviews and reports,* vol. 15, p. 814–826, 2019.

[48] M. S. Dicken, A. R. Hughes and S. T. Hentges, "Gad1 mRNA as a reliable indicator of altered GABA release from orexigenic neurons in the hypothalamus.," *The European journal of neuroscience,* vol. 42, no. 9, p. 2644–2653, November 2015.

[49] Z. Z. Pan, "Transcriptional control of Gad2.," *Transcription,* vol. 3, no. 2, p. 68–72, 2012.

[50] O. M. Schlüter, J. Basu, T. C. Südhof and C. Rosenmund, "Rab3 superprimes synaptic vesicles for release: implications for short-term synaptic plasticity.," *The Journal of neuroscience : the official journal of the Society for Neuroscience,* vol. 26, no. 4, p. 1239–1246, January 2006.

[51] T. Tsetsenis, T. J. Younts, C. Q. Chiu, P. S. Kaeser, P. E. Castillo and T. C. Südhof, "Rab3B protein is required for long-term depression of hippocampal inhibitory synapses and for normal reversal learning," *Proceedings of the National Academy of Sciences,* vol. 108, p. 14300–14305, 2011.

[52] 10x Genomics, "Human Kidney Preview Data (Xenium Human Multi-Tissue and Cancer Panel)," *In Situ Gene Expression dataset analyzed using Xenium Onboard Analysis 1.5.0,* 2023, July 17.

[53] 10x Genomics, "Xenium In Situ Analysis of Alzheimer's Disease Mouse Model Brain Coronal Sections from One Hemisphere Over a Time Course," *In Situ Gene Expression dataset analyzed using Xenium Onboard Analysis 1.4.0,* 2023, July 13.

[54] G. Novikova, M. Kapoor, J. Tcw, E. M. Abud, A. G. Efthymiou, S. X. Chen, H. Cheng, J. F. Fullard, J. Bendl, Y. Liu and others, "Integration of Alzheimer's disease genetics and myeloid genomics identifies disease risk regulatory elements and genes," *Nature communications,* vol. 12, p. 1610, 2021.

[55] S. Baig, S. A. Joseph, H. Tayler, R. Abraham, M. J. Owen, J. Williams, P. G. Kehoe and S. Love, "Distribution and expression of picalm in Alzheimer disease.," *Journal of neuropathology and experimental neurology,* vol. 69, no. 10, p. 1071–1077, October 2010.

[56] W. Xu, L. Tan and J.-T. Yu, "The Role of PICALM in Alzheimer's Disease.," *Molecular neurobiology,* vol. 52, no. 1, p. 399–413, August 2015.

[57] W. Xu, H.-F. Wang, L. Tan, M.-S. Tan, C.-C. Tan, X.-C. Zhu, D. Miao, W.-J. Yu, T. Jiang, L. Tan and others, "The impact of PICALM genetic variations on reserve capacity of posterior cingulate in AD continuum," *Scientific reports,* vol. 6, p. 24480, 2016.

[58] 10x Genomics, *Exploring Alzheimer's-like pathology at subcellular resolution using Xenium In Situ.*

[59] J. Yang, Z. Fu, X. Zhang, M. Xiong, L. Meng and Z. Zhang, "TREM2 ectodomain and its soluble form in Alzheimer's disease.," *Journal of neuroinflammation,* vol. 17, no. 1, p. 204, July 2020.

[60] L.-F. Lue, C. T. Schmitz, G. Serrano, L. I. Sue, T. G. Beach and D. G. Walker, "TREM2 Protein Expression Changes Correlate with Alzheimer's Disease Neurodegenerative Pathologies in Post-Mortem Temporal Cortices.," *Brain pathology (Zurich, Switzerland),* vol. 25, no. 4, p. 469–480, July 2015.

[61] Q. Qin, Z. Teng, C. Liu, Q. Li, Y. Yin and Y. Tang, "TREM2, microglia, and Alzheimer's disease.," *Mechanisms of ageing and development,* vol. 195, p. 111438, April 2021.

[62] E. Papuć and K. Rejdak, "The role of myelin damage in Alzheimer's disease pathology.," *Archives of medical science : AMS,* vol. 16, no. 2, p. 345–351, 2020.

[63] S. Ruskamo, A. Raasakka, J. S. Pedersen, A. Martel, K. Škubník, T. Darwish, L. Porcar and P. Kursula, "Human myelin proteolipid protein structure and lipid bilayer stacking," *Cellular and Molecular Life Sciences,* vol. 79, p. 419, 2022.

[64] P. Montague, A. S. McCallion, R. W. Davies and I. R. Griffiths, "Myelin-associated oligodendrocytic basic protein: a family of abundant CNS myelin proteins in search of a function," *Developmental neuroscience,* vol. 28, p. 479–487, 2006.

[65] M. Gravel, B. Trapp, J. Peterson and P. E. Braun, "CNP in myelination: Overexpression alters oligodendrocyte morphogenesis," *Cell Biology and Pathology of Myelin: Evolving Biological Concepts and Therapeutic Approaches,* p. 75–82, 1997.

[66] R. R. Sturrock, "Myelination of the mouse corpus callosum," *Neuropathology and applied neurobiology,* vol. 6, p. 415–420, 1980.

[67] M. Ota, N. Sato, Y. Kimura, Y. Shigemoto, H. Kunugi and H. Matsuda, "Changes of myelin organization in patients with Alzheimer's disease shown by q-space myelin map imaging," *Dementia and Geriatric Cognitive Disorders Extra,* vol. 9, p. 24–33, 2019.

[68] S. Das, M. Vera, V. Gandin, R. H. Singer and E. Tutucci, "Intracellular mRNA transport and localized translation," *Nature reviews Molecular cell biology,* vol. 22, p. 483–504, 2021.

[69] H. Mi, D. Ebert, A. Muruganujan, C. Mills, L.-P. Albou, T. Mushayamaha and P. D. Thomas, "PANTHER version 16: a revised family classification, tree-based classification tool, enhancer regions and extensive API," *Nucleic acids research,* vol. 49, p. D394–D403, 2021.

[70] T. Biancalani, G. Scalia, L. Buffoni, R. Avasthi, Z. Lu, A. Sanger, N. Tokcan, C. R. Vanderburg, Å. Segerstolpe, M. Zhang and others, "Deep learning and alignment of spatially resolved single-cell transcriptomes with Tangram," *Nature methods,* vol. 18, p. 1352–1362, 2021.

[71] S. M. Lundberg and S.-I. Lee, "A Unified Approach to Interpreting Model Predictions," in *Advances in Neural Information Processing Systems 30*, I. Guyon, U. V. Luxburg, S. Bengio, H. Wallach, R. Fergus, S. Vishwanathan and R. Garnett, Eds., Curran Associates, Inc., 2017, p. 4765–4774.

[72] S. M. Lundberg, G. Erion, H. Chen, A. DeGrave, J. M. Prutkin, B. Nair, R. Katz, J. Himmelfarb, N. Bansal and S.-I. Lee, "From local explanations to global understanding with explainable AI for trees," *Nature Machine Intelligence,* vol. 2, pp. 2522-5839, 2020.

[73] E. Welzl, "Smallest enclosing disks (balls and ellipsoids)," in *New Results and New Trends in Computer Science: Graz, Austria, June 20–21, 1991 Proceedings*, 2005.

[74] S. Seabold and J. Perktold, "statsmodels: Econometric and statistical modeling with python," in *9th Python in Science Conference*, 2010.

[75] F. A. Wolf, P. Angerer and F. J. Theis, "SCANPY: large-scale single-cell gene expression data analysis," *Genome biology,* vol. 19, p. 1–5, 2018.

[76] N. Rezaie, F. Reese and A. Mortazavi, "PyWGCNA: a Python package for weighted gene co-expression network analysis," *Bioinformatics,* vol. 39, p. btad415, 2023.

[77] V. A. Padilha and R. J. G. B. Campello, "A systematic comparative evaluation of biclustering techniques," *BMC bioinformatics,* vol. 18, p. 1–25, 2017.

675
676

## Figure Legends

**Figure 1: Schematic of CellSP. (A)** CellSP analyzes single-molecule resolution spatial transcriptomics data from a tissue; such data provides subcellular locations of individual transcripts of a set of genes within each delineated cell. **(B)** Subcellular Pattern Discovery. CellSP utilizes existing tools InSTAnT and SPRAWL for the discovery of subcellular spatial patterns of genes within each cell. Types of patterns detected include gene-gene co-localization reported by InSTAnT and four types of subcellular localization preferences (peripheral, punctate, central, radial) reported by SPRAWL. **(C)** Module Discovery. The next step identifies spatial patterns involving multiple genes and cells. Patterns identified in the previous step (represented as matrices of cells x genes or gene-pairs) are subjected to a biclustering analysis that identifies a subset of rows and columns with a large average value, representing a "gene-cell module": a set of genes or gene-pairs exhibiting the same subcellular pattern within the same cells. Gene-cell modules that overlap in a significant number of genes (or gene pairs) are coalesced to reduce redundancy. This step outputs a set of gene-cell modules with varying number of cells and genes. **(D)** CellSP provides intuitive visualizations of gene-cell modules, which often span tens to hundreds of cells making direct inspection impractical. CellSP visualizations are tailored to the type of pattern defining the module and summarize the strength of subcellular spatial pattern involving module-associated genes and cells while contrasting them with background genes and cells. **(E)** Module Characterization. Module-associated genes are subjected to Gene Ontology (GO) analysis to gain functional insights into detected gene-cell modules. Alternatively, a Random Forest classifier is trained to differentiate module cells from non-module cells and the most predictive genes, called cell-marker genes, are subjected to GO analysis. To address the limited size of gene panels in subcellular spatial transcriptomic datasets, CellSP employs Tangram to impute gene expression from single-cell RNA-seq datasets of the same tissue, enabling more comprehensive analysis. Results of GO analysis are visualized using REVIGO plots.

**Figure 2**: **CellSP reveals myelination-related subcellular spatial phenomena in mouse brain. (A)** Summary table of an example gene-cell module, "M0_I", discovered by CellSP from MERFISH data on hypothalamic preoptic area in mouse brain. (The suffix "_I" indicates that it was discovered by aggregating single-cell level colocalization patterns reported by InSTAnT.) "GO Genes" shows the Gene Ontology (GO)-based characterization of the four module genes. "GO Cells" shows the GO-based characterization of the genes whose expression levels are most discriminative of the 332 module cells versus remaining cells. **(B)** Direct visualization of six of the 332 module cells, with blue boundaries indicating automatically delineated cell periphery, red boundaries indicating nuclear periphery, each dot representing a transcript, colored in green for module genes and in gray for other genes. **(C)** CellSP visualization of module M0_I. The heatmap shows pairwise colocalization propensity of gene pairs in module cells compared to non-module cells, as a log ratio, with warmer colors (more positive values) indicating specificity of the colocalization to the module cells. The first half of rows and columns corresponds to module genes while the second half corresponds to a random subset of non-module genes, so the contrast between the upper left quadrant (more warm color cells) and other quadrants underscores that the phenomenon is specific to the module gene pairs. **(D)** UMAP visualization of all cells in the sample, with colors indicating cell types and module cells shown in black. The module mostly comprises mature oligodendrocytes (ODM). **(E)** REVIGO plot of biological processes enriched in module genes, showing a prominent association with myelination-related terms. **(F)** REVIGO plot of biological processes associated with gene markers of module cells, showing that these cells are also characterized by genes enriched for myelination-related terms.

**Figure 3: CellSP reveals axonogenesis related subcellular spatial phenomena in mouse brain. (A)** Summary table of an example gene-cell module, "M0_S", discovered by CellSP from

MERFISH data on hypothalamic preoptic area in mouse brain. (The suffix "_S" indicates that it was discovered by aggregating single-cell level colocalization patterns reported by SPRAWL.) **(B)** Direct visualization of six of the 221 module cells, with each dot representing a transcript, colored in green for module genes and in gray for other genes. **(C)** CellSP visualization of module M0_S. The subcellular space is idealized as a circle with concentric rings representing varying distances from the "center" (see Methods) and color intensity representing transcript density averaged over the module cells. The upper circle depicts this information for module genes and the lower circle represents all other genes for contrast, which in this case highlights that the module gene transcripts are enriched in peripheral regions (outermost ring). This type of visualization is used for any gene-cell module with peripheral or central pattern. **(D)** UMAP visualization of all cells in the tissue, with colors indicating cell types and module cells shown in black. The module mostly comprises neurons. **(E)** REVIGO plot of biological processes associated with module genes, highlighting enrichment for axonogenesis-related terms. **(F)** REVIGO plot of biological processes associated with marker genes of module cells, showing that these cells are characterized by genes enriched for cell adhesion-related terms. **(G-H)** Spatial plot of all cells in tissue (H) with module cells highlighted in red, along with detailed visualization of a subset of module cells in close spatial proximity (G,I). In these detailed views, module cells are depicted with a stronger boundary, while their fill color corresponds to their cell type. Transcripts of module genes are highlighted in red and are localized at the contact boundaries between module cells.

**Figure 4**: **CellSP uncovers myelination and GABA-ergic synpase related modules across cell types and regions of mouse brain. (A)** UMAP visualization of all cells in a Xenium data set of whole mouse brain, with cells of 36 myelination-related gene-cell modules detected by CellSP shown in color. (Cells of each module are shown in a different color.) This demonstrates that CellSP captures myelination-related subcellular patterns across cells with diverse gene expression profiles, indicating that these patterns are not merely a reflection of overall gene expression levels. **(B)** Spatial plot of all cells in the whole brain data set, with cells of myelination-related modules (same as in A) shown in different colors, while cells not in any of these modules are shown in grey. **(C)** Matrix showing gene composition of each of the 36 myelination-related modules (rows); blue indicates a gene's inclusion in a module. Genes Sox10, Gjc3, and Opalin appear in all or most modules, while four others appear in a majority of modules. **(D)** REVIGO plot of biological processes associated with module genes, aggregated over all 36 modules. Color intensity represents the number of modules for which a GO term is significantly associated with module genes. **(E)** REVIGO plot of biological processes associated with gene markers of module cells, aggregated over all the 36 modules. **(F)** UMAP visualization of all cells in data set, with cells in any of the 20 discovered GABA-ergic synapse-related modules shown in color. (Cells of each module are shown in a different color.) **(G)** Spatial plot of all cells in the sample, with cells from all 20 GABA-ergic synapse-related modules shown in different colors, while cells not in any of these modules are shown in grey.

**Figure 5**: **CellSP detects differences in subcellular spatial patterns between tissue conditions. (A)** Spatial plot of a Kidney PRCC (kidney cancer) tissue (Xenium data), highlighting cluster 6 cells in blue, cluster 9 cells in green, and cells of any of the 6 CellSP-detected immune-response related gene-cell modules in red. **(B, C, D)** CellSP visualization of three selected immune system related gene-cell modules discovered in the cancer sample. B shows module R6_M5_S (central pattern) in left panel while right panel is a visualization of the subcellular distribution of the module genes in expression-matched cells from the healthy kidney sample ("control"). Module genes are more uniformly localized towards the cell's "center" in the cancer sample than in healthy sample. C shows module R6_M0_S (radial pattern) in left panel and the right panel depicts the subcellular distribution of module genes in cells from the healthy sample. The cancer sample (left panel) shows a strong clear difference between module genes and non-

module genes in terms of radial spread of transcripts, while this contrast is insignificant in the healthy sample (right panel). D shows module R6_M3_I, defined by a colocalization pattern. The colocalization visualization has been modified to provide contrast with control cells rather than non-module cancer cells. The module genes are much more proximal to each other in cancer module cells than in random cells from the healthy sample. **(E)** Gene-cell modules detected in mouse hemibrain Xenium samples from three TgCRND8 mice (AD model) at different time points and three wildtype (WT) mice at similar time points were examined for inclusion of six AD-related genes (columns). Shown are the number of detected modules in each of the six samples (rows) that include a gene. Notably, Picalm and Trem2 have more modules detected in AD samples than in WT, consistent with their known roles in Alzheimer's Disease-related processes. **(F)** Chord diagram depicting the number of modules detected in AD samples (bottom) or WT samples (top) that include a pair of genes, shown for genes annotated with function "ensheathment of neurons". The gene pairs "Olig2-Plp1" and "Olig2-Mobp" (shown in black) exhibit a significant difference between AD and WT samples. **(G)** Blue bars show z-scores computed from a proportion test comparing AD and WT samples in terms the fraction of CellSP modules that include Olig2 and another gene (x-axis labels), shown only for partner genes where the proportion test yields a significant p-value. Orange bars show similarly calculated z-scores for modules defined by cell-level co-expression, as computed by WGCNA.

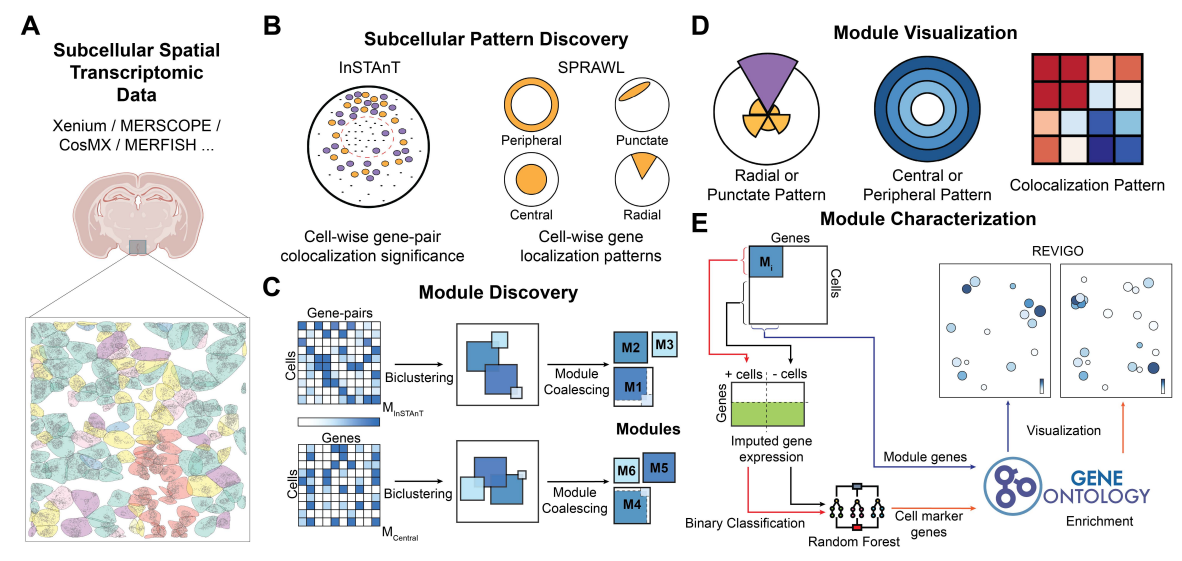
A
Subcellular Spatial Transcriptomic Data
Xenium / MERSCOPE / CosMX / MERFISH ...
B
Subcellular Pattern Discovery
InSTAnT
SPRAWL
Peripheral
Punctate
Central
Radial
Cell-wise gene-pair colocalization significance
Cell-wise gene localization patterns
C
Module Discovery
Gene-pairs
Cells
Biclustering
Module Coalescing
M2
M3
M1
Genes
Modules
M6
M5
M4
D
Module Visualization
Radial or Punctate Pattern
Central or Peripheral Pattern
Colocalization Pattern
E
Module Characterization
Genes
Cells
REVIGO
+ cells ; - cells
Imputed gene expression
Module genes
Visualization
GENE ONTOLOGY
Enrichment
Binary Classification
Random Forest
Cell marker genes

A

| Module 0 InSTAnT | |
|---|---|
| #Genes | 4 |
| #Cells | 332 |
| Genes | Sgk1,Ttyh2,Ermn, Ndrg1 |
| GO Genes | Cytoskeletal protein bind. |
| GO Cells | Myelination |

B

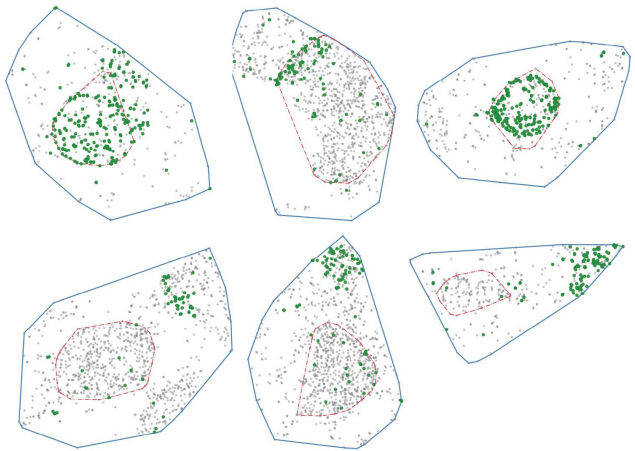

C

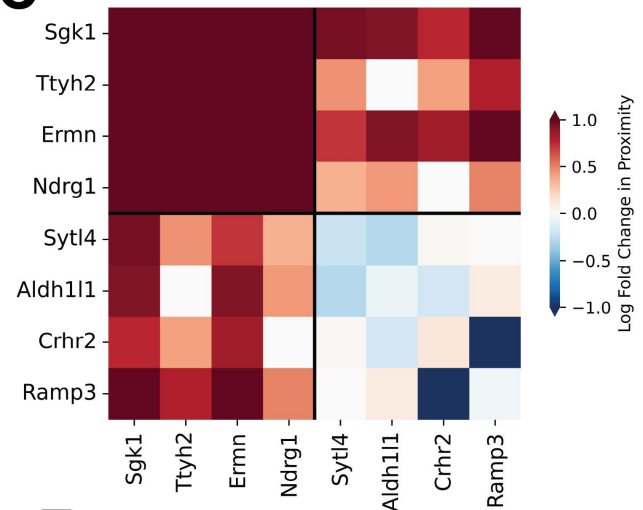


D

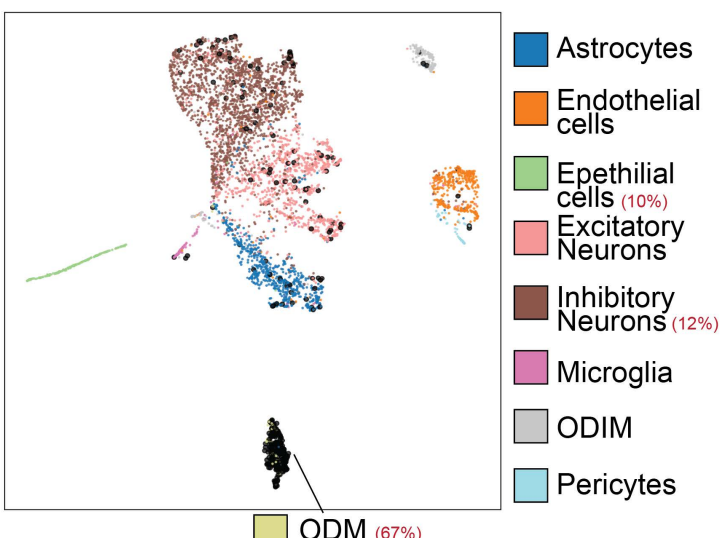


E

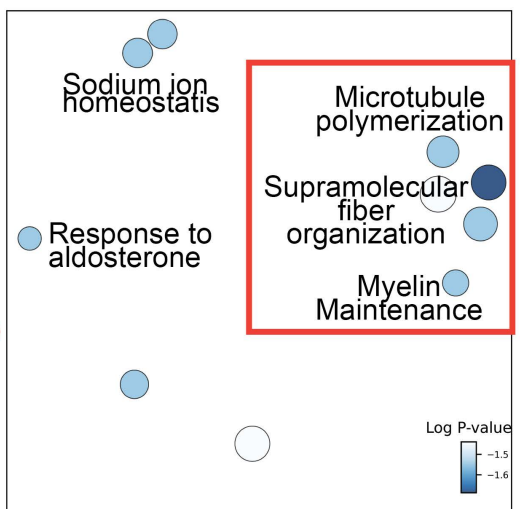


F

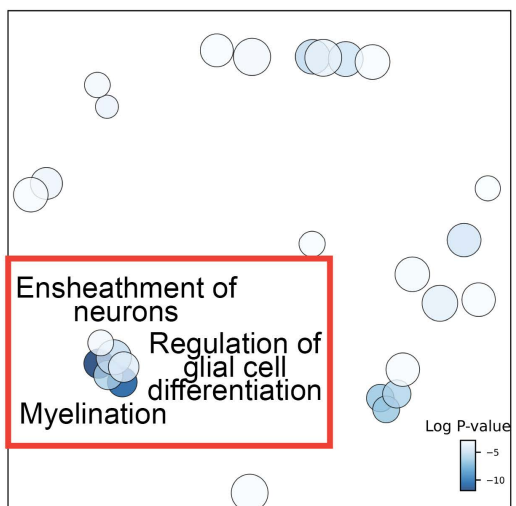

A

| Module 0 SPRAWL | |
|---|---|
| #Genes | 4 |
| #Cells | 221 |
| Pattern | Peripheral |
| Genes | Fn1,Slco1a4,Rgs5,Sema3c |
| GO Genes | Regulation of axon extension |
| GO Cells | Cell-Cell adhesion |

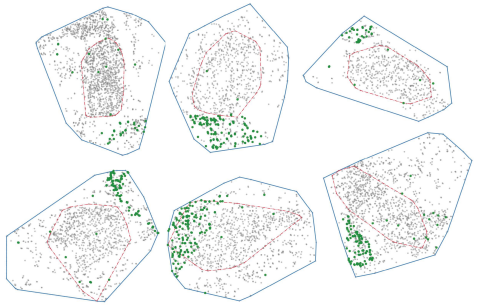


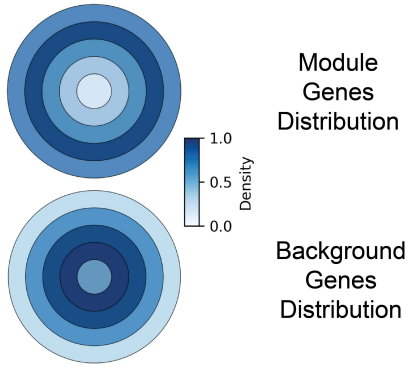


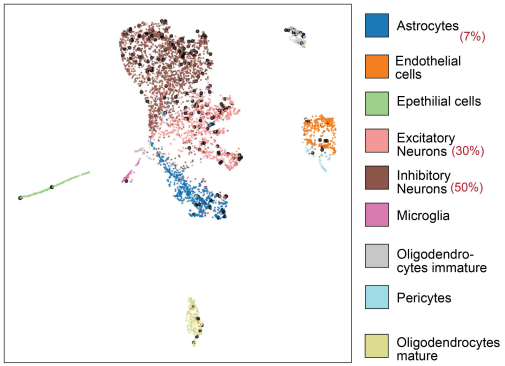


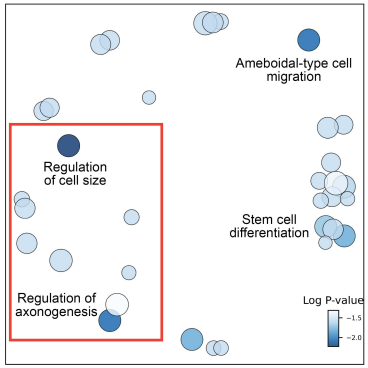


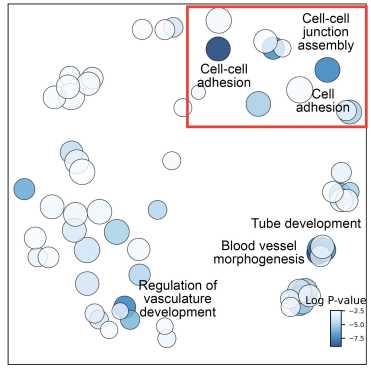


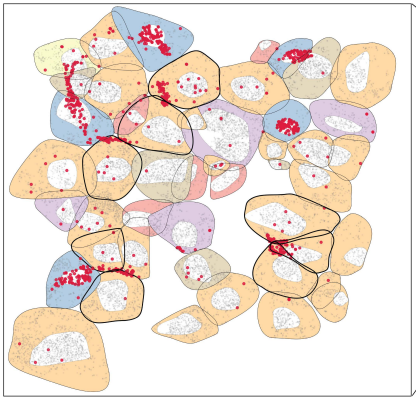


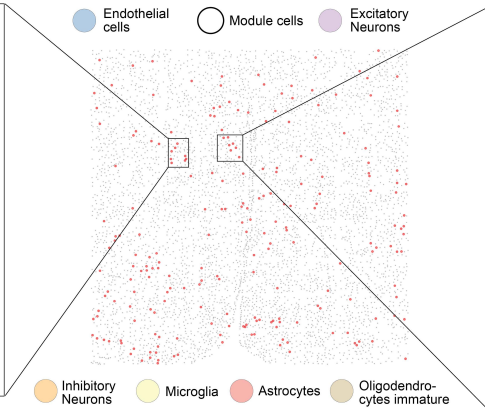


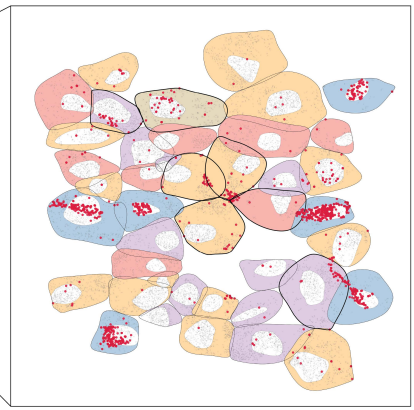

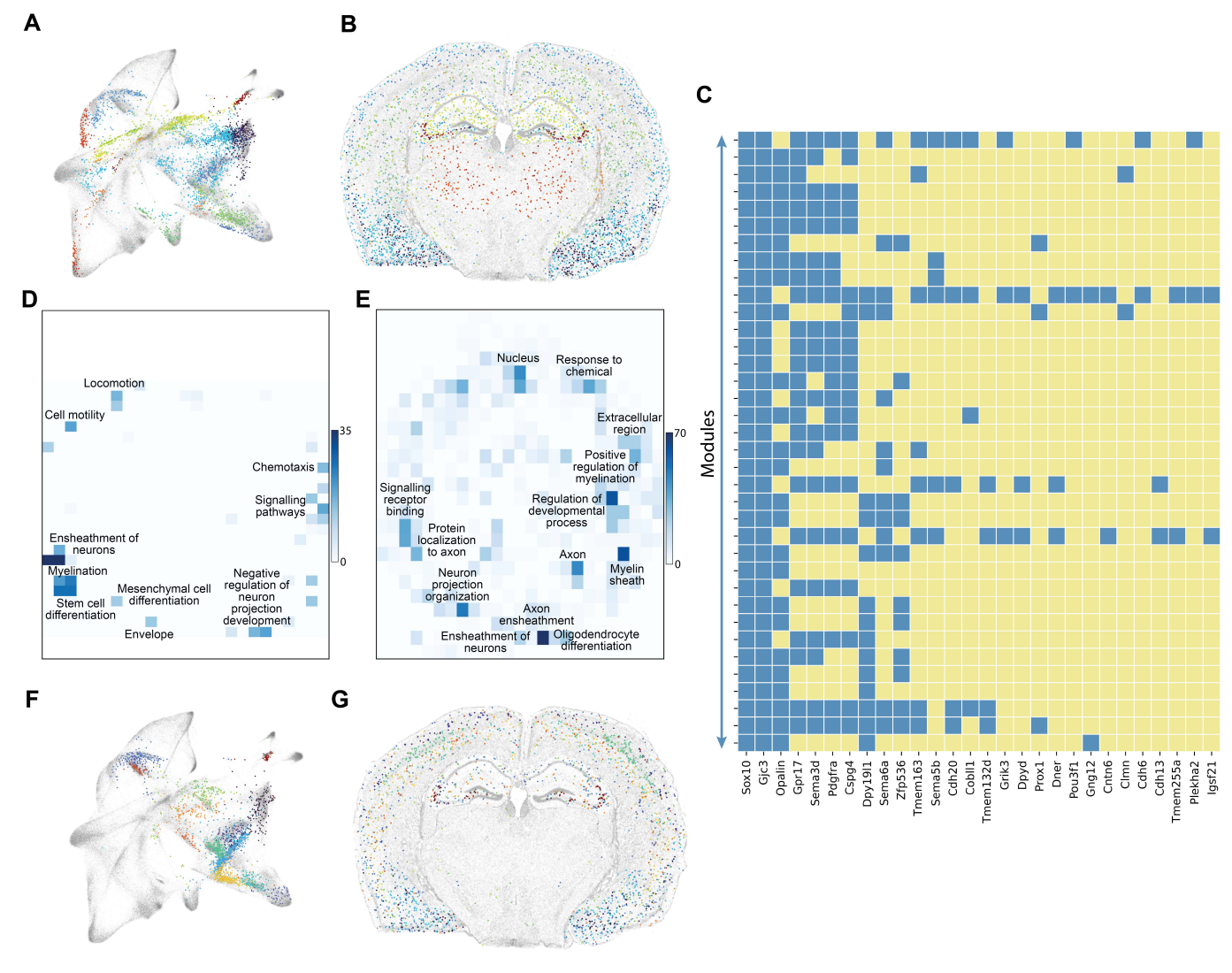
A
B
C
D
E
F
G
Modules
Locomotion
Cell motility
Chemotaxis
Signalling pathways
Ensheathment of neurons
Myelination
Stem cell differentiation
Mesenchymal cell differentiation
Envelope
Negative regulation of neuron projection development
35
0
Nucleus
Response to chemical
Extracellular region
Positive regulation of myelination
Signalling receptor binding
Regulation of developmental process
Protein localization to axon
Axon
Myelin sheath
Neuron projection organization
Axon ensheathment
Ensheathment of neurons
Oligodendrocyte differentiation
70
0
Sox10
Gjc3
Opalin
Gpr17
Sema3d
Pdgfra
Cspg4
Dpy19l1
Sema6a
Zfp536
Tmem163
Sema5b
Cdh20
Cobll1
Tmem132d
Grik3
Dpyd
Prox1
Dner
Pou3f1
Gng12
Cntn6
Clmn
Cdh6
Cdh13
Tmem255a
Plekha2
Igsf21

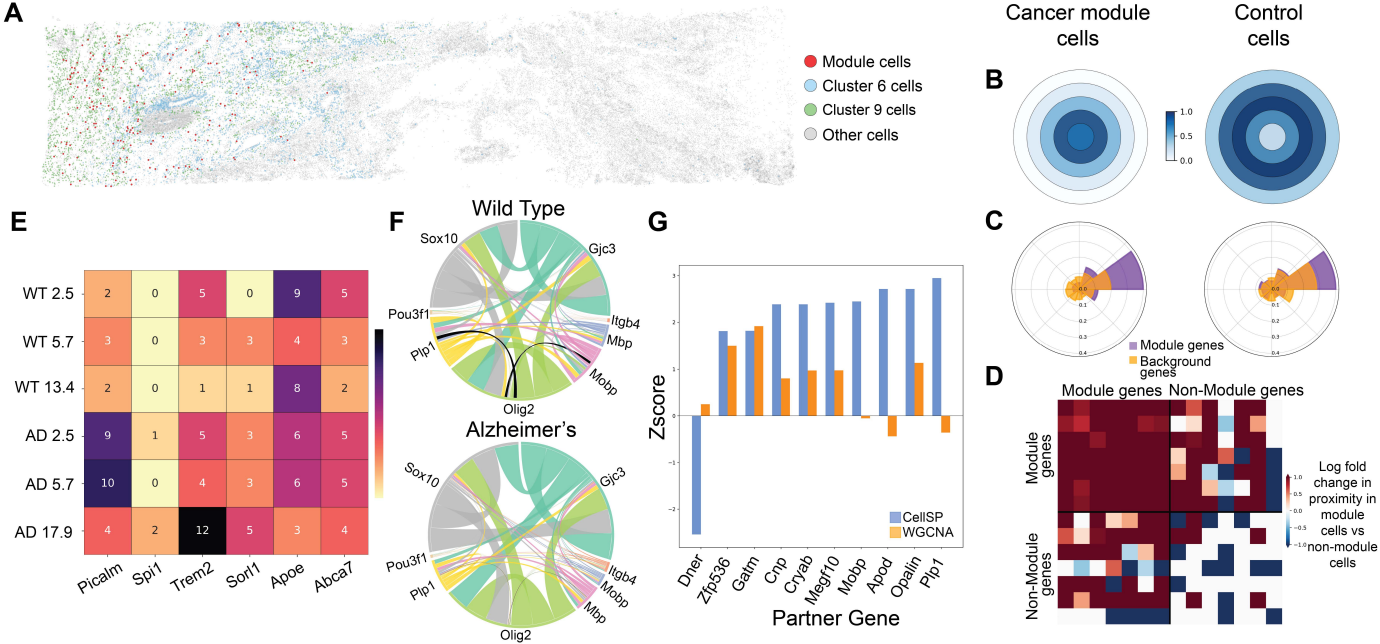
A
Module cells
Cluster 6 cells
Cluster 9 cells
Other cells
Cancer module cells
Control cells
B
1.0
0.5
0.0
C
Module genes
Background genes
D
Module genes
Non-Module genes
Module genes
Non-Module genes
Log fold change in proximity in module cells vs non-module cells
E
WT 2.5
WT 5.7
WT 13.4
AD 2.5
AD 5.7
AD 17.9
Picalm
Spi1
Trem2
Sorl1
Apoe
Abca7
F
Wild Type
Alzheimer's
Sox10
Gjc3
Pou3f1
Itgb4
Plp1
Mbp
Mobp
Olig2
G
Zscore
CellSP
WGCNA
Dner
Zfp536
Galm
Cnp
Cryab
Megf10
Mobp
Apod
Opalin
Plp1
Partner Gene